

## ZnO-Loaded SA-g-Poly (AC-co-EBS) Hydrogel Nanocomposite as an Efficient Adsorption of Tetracycline and Phenol: Kinetics and Thermodynamic Models

Aseel Mushtak Aljeboree<sup>1</sup>, Mohammed Kassim Al-Hussainawy<sup>2\*</sup>, Usama Salim Altimari<sup>3</sup>, Shaymaa Abed Al-Hussein<sup>4</sup>, Maha Daham Azeez<sup>5</sup>, and Ayad Fadhil Alkaim<sup>1</sup>

<sup>1</sup>Department of Chemistry, College of Sciences for Girls, University of Babylon, Hilla 51001, Iraq

<sup>2</sup>Ministry of Education, Directorate of Education Al-Muthanna, Al-Samawah, AL-Muthanna 66001, Iraq

<sup>3</sup>Department of Medical Laboratories Technology, AL-Nisour University College, Baghdad 10017, Iraq

<sup>4</sup>Department of Medical Laboratories Technology, Al-Manara College for Medical Sciences, Maysan 62001, Iraq

<sup>5</sup>National University of Science and Technology, Dhi Qar 64001, Iraq

\* **Corresponding author:**

email: kassim1316@gmail.com

Received: July 9, 2023

Accepted: October 10, 2023

DOI: 10.22146/ijc.86711

**Abstract:** A synthetic superabsorbent polymer hydrogel nanocomposite was prepared by the free radical graft co-polymerization method. This study included the preparation of two surfaces: first sodium alginate-g-(acrylic acid-co-sodium; 4-ethenylbenzenesulfonate), SA-g-poly (Ac-co-EBS) hydrogel, and second surface hydrogel after zinc oxide loading SA-g-poly (Ac-co-EBS). Hydrogel nanocomposite was prepared from different monomers for the removal of pollutants. The physical characterizations of nanocomposite have been studied using several techniques like UV-vis, FTIR, FE-SEM, TEM, EDX, and XRD. The data from the adsorption study show that E% increases with increasing contact time, with the best agitation time of 1 h, after which the adsorption becomes constant. The increase in adsorbent amount 0.01–0.1 g, the percentage removal of tetracycline (TC) and phenol (PH) increased from 60.639–97.085 and 487.71–94.05%, respectively, and  $Q_e$  decreased 606.39–97.08 to 487.1831–94.456 mg/g on hydrogel. The  $\Delta H$  value is endothermic. All processes of adsorption are considered spontaneous, from a negative value of  $\Delta G$  to a positive value of  $\Delta S$ . The release of the TC drug was studied in conditions similar to those in the human body in terms of acidity and temperature. The cumulative release of TC drug in 3 h was 50.65%, 42.33%, pH = 7.5 and pH 1.2, respectively.

**Keywords:** kinetics; thermodynamic; hydrogel; adsorption; tetracycline; phenol

### ■ INTRODUCTION

Pharmaceuticals are chemicals commonly used in the treatment and diagnosis of diseases. Also, they are used to include veterinary compounds applied to illegal drugs [1]. Pharmaceuticals are produced in very large quantities and consume a variety of drugs that are used in the treatment of mankind, including synthetic hormones, statins, antibiotics, cytotoxins, and anti-inflammatories [2-4]. Tetracycline (TC) has been most utilized in human treatment and husbandry animals, with a global yearly production of more than 20,000 tons; thus, it has been one of the most repeatedly discovered antibiotics in

wastewater [5]. Utilized to treat a number of infections, including acne, malaria, brucellosis, cholera, plague, and syphilis. Common side effects include vomiting, rash, diarrhea, and loss of appetite. TC has a formula of  $C_{22}H_{24}N_2O_8$  with a molecular weight of 444.4 g/mol [6].

Phenol (PH, also called carbolic acid, phenylic acid hydroxybenzene) is also a common water pollutant, and it is considered a carcinogen and a danger to human health, even at low concentrations. Therefore, the treatment of industrial water containing PH has become necessary. PH is an aromatic organic compound with the molecular formula  $C_6H_5OH$ . It is a white crystalline solid that is volatile. The molecule consists of a phenyl

group ( $-C_6H_5$ ) bonded to a hydroxy group ( $-OH$ ) with a mildly acidic, molecular weight of 49.113 g/mol,  $\lambda_{max} = 270$  nm, and IUPAC name of benzenol. PH and its chemical derivatives are essential for the production of polycarbonates, epoxies, bakelite, nylon, detergents, herbicides such as phenoxy herbicides, and numerous pharmaceutical drugs [7-8].

The presence of zinc oxide (ZnO) nanoparticles as additives to the polymers leads to an increase in the surface area and a high loading rate of the materials, in addition to an increase in selectivity and low toxicity, making them ideal systems for increasing the loading of some pollutants from aqueous solutions after the polymers were suffering from a decrease in their effectiveness. That can be achieved by increasing the nanofillers, which will give a better solution to get rid of the problem of weak polymers in terms of durability, selectivity, and surface charge [9-10]. ZnO nanoparticles and other nanoparticles are also widely used in various fields because of their distinctive physical and chemical properties. They have been widely used recently in the polymer industry, as they can provide corrosion resistance to polymer composites and improve the polymer's high performance in terms of hardness, weight, and aging resistance [11].

Hydrogels and their composites are currently considered one of the methods used to remove industrial pollutants that directly affect the environment and humans by means of adsorption technology [12], which has the ability to swell and control the controlled delivery of drugs, so many researchers have used hydrogels and their composites to remove water contaminants such as dyes, drugs, and organic compounds by adsorption, among wastewater treatments such as oxidation processes (which include photolysis and ultrasonic decomposition) and conventional methods (reverse osmosis and membrane separation). The adsorption technique is one of the methods used to remove pollutants because of its ease of application, high efficiency, and the possibility of returning the adsorbed materials to the solution by controlled release [13].

The study of kinetics and thermodynamics is one of the important measurements to find out the time period

to reach the equilibrium state of the adsorbed contaminated materials at which the adsorption process depends, while thermodynamics was studied to know if the adsorption process was exothermic or endothermic before and after the addition of the nanomaterial and to know the direction of the reaction and the nature of powers and an indication of their importance for comparison in studies.

In this investigation, experimental variables like pH, concentration, and temperature were examined in order to better understand the TC and PH adsorption capabilities of hydrogels. The adsorption isotherm, kinetic, and thermodynamic parameters have been computed from the experiment findings.

## ■ EXPERIMENTAL SECTION

### Materials

The materials used in this study were sodium-4-ethenylbenzenesulfonate hydrate (EBS, 99%); acrylic acid (Ac, 98%); potassium persulphate (KPS, 98%), sodium alginate (SA), *N,N*-dimethyl acrylamide (MBA, 96%), and ZnO, where all analytical chemicals are of high purity and were used directly without further purification and all obtained from Sigma Aldrich (China, Shanghai). TC (91%) and PH (99%) are getting from Sigma-Aldrich (Overijse, Belgium).

### Instrumentation

The instrumentations used in this study were UV-vis spectrophotometers (Perkin Elmer, Lambda 35), X-ray diffraction spectroscopy (S-4800, Hitachi, Japan), KBr disks ( $4000-400$   $cm^{-1}$ ), FTIR spectroscopy (8400S, Shimadzu, Japan). Field emission scanning electron microscope (FE-SEM, MIRA3, TESCAN, Iran) with an accelerating voltage of 15 kV and transmission electron microscopy (TEM) (MIRA3, TESCAN, Iran).

### Procedure

#### **Adsorption experimental**

The adsorption technique was studied using adsorption parameters such as the concentration of the pollutants at a time. All experiments on adsorption and drug delivery have studied kinetic and isotherm parameters through UV-vis spectrophotometer. The

results were followed up by plotting the amount of the adsorbent against the concentration of the adsorbent and knowing its effect on the adsorption process. The amount of adsorbent was found using the Eq. (1);

$$Q_e = \frac{V_{\text{sol}}(C_0 - C_e)}{m} \quad (1)$$

where  $C_0$  and  $C_e$  are TC and PH concentrations (ppm) at the initial concentration and equilibrium time, respectively.  $Q_e$  ( $\text{mg g}^{-1}$ ) is the amount of TC and PH adsorbed on the hydrogel adsorbent (g).  $V$  is the volume in the liter unit.

### Preparation of ZnO-loaded SA-g-poly (Ac-co-EBS) hydrogel nanocomposite

The free radical graft copolymerization method is based on the preparation of super adsorption and swelling hydrogel by dissolving 1 g of SA in 20 mL of distilled water. The magnetic bar was used to stir until bubbles were removed, and then 0.1 g of ZnO NPs was dispersed in 20 mL of distilled water and shaken ultrasonically for 30 min. Then, it was gradually added to the SA solution, followed by stirring at 25 °C for 2 h until a homogeneous gel was dispersed. At this point, 0.5 g of EBS was added, followed by 3 mL of AC, and consistent mixing at 25 °C was performed. Then 0.03 g of KPS was added to 1 mL distilled water with continuous mixing for 5 min. Next, 0.05 g of MBA was added to the mixture after  $\text{N}_2$  was purged. It was finally set in a water bath at 70 °C to complete the co-polymerization reaction and obtain the ZnO-loaded SA-g-poly (Ac-co-EBS) hydrogel nanocomposite, as shown in Fig. 1.

## RESULTS AND DISCUSSION

### Characterization

FTIR of SA-g-poly (Ac-co-EBS) and SA-g-poly (Ac-co-EBS)/ZnO hydrogel composites were investigated before and after adsorption of TC drug and PH pollutants (Fig. 2). Also, the absorption bands and their vibrations are summarized by FTIR bands of SA, Ac, and EBS. The grafting of Ac is supported via a new characteristic adsorption band  $1718 \text{ cm}^{-1}$ , assigned to  $\text{C}=\text{O}$  stretching in the spectrum of ZnO-loaded SA-g-poly (Ac-co-EBS) hydrogel nanocomposite. The amalgamation of ZnO NPs in the structure of the composite, the bands indicate the

interaction among ZnO hydrogen and nitrogen atoms to result in the Zn–O bond at around  $460\text{--}490 \text{ cm}^{-1}$ . The hydroxyl group (O–H) of acrylic acid and alginate-stretching vibration caused all the hydrogels to exhibit a recognizable wide-stretching frequency at  $3000\text{--}3500 \text{ cm}^{-1}$ . A weak band with several peaks at  $1040, 1113, 1236,$  and  $1262 \text{ cm}^{-1}$  is ascribed to alcohols, carboxylic acids, and ethers ( $1000\text{--}1320 \text{ cm}^{-1}$  is attributed to C–O stretch), while a prominent peak at  $1713\text{--}1725 \text{ cm}^{-1}$  is indexed to the carbonyl group ( $\text{C}=\text{O}$ ) stretching vibration for all components [14–16]. After the adsorption of TC and PH, we find the expansion of the bands due to the presence of an abundance of drug hydroxyls, the occurrence of electrostatic attraction, and the effect of van der Waals forces [17].

### X-Ray Diffraction Patterns

XRD patterns of both SA-g-poly (Ac-co-EBS) hydrogel, ZnO-loaded SA-g-poly (Ac-co-EBS) hydrogel composite, and ZnO NPs are shown in Fig. 3, which indicates that SA-g-poly (Ac-co-EBS) is amorphous, but ZnO-loaded SA-g-poly (Ac-co-EBS) hydrogel composite appears to be crystalline materials that net from the peaks present in the broadband of a nanocomposite at  $36.6^\circ$  [18–19]. These analysis results showed that the sample as well as the synthesis results, had a low crystal phase purity. The crystallographic structure of SA-g-poly (Ac-co-EBS) composites was changed by using a



**Fig 1.** Image of a superabsorbent ZnO-loaded SA-g-poly (Ac-co-EBS) hydrogel composite

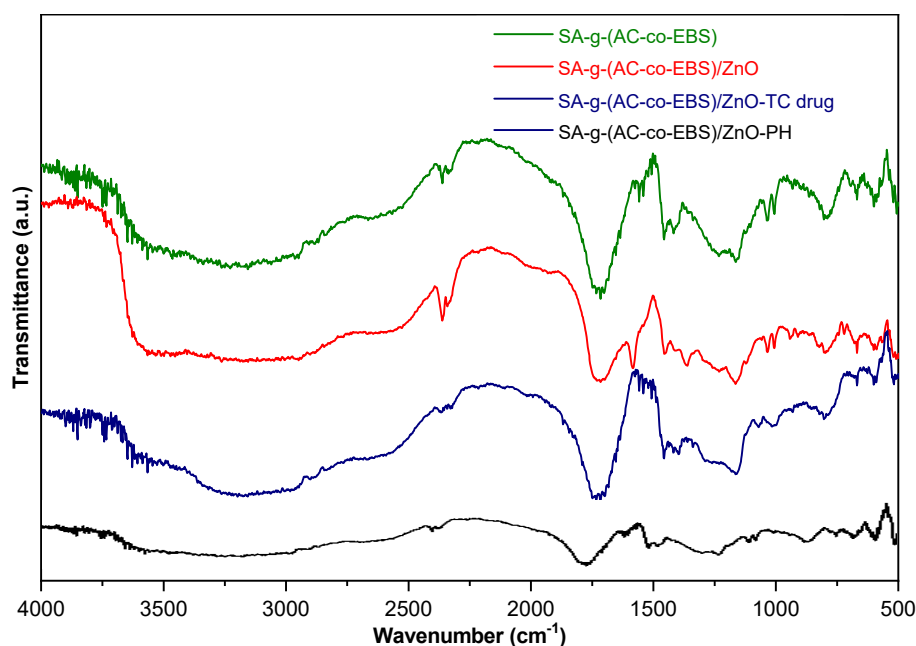


Fig 2. FTIR spectra of before and after adsorption of TC and PH ( $40 \text{ mg. L}^{-1}$  both TC and PH)

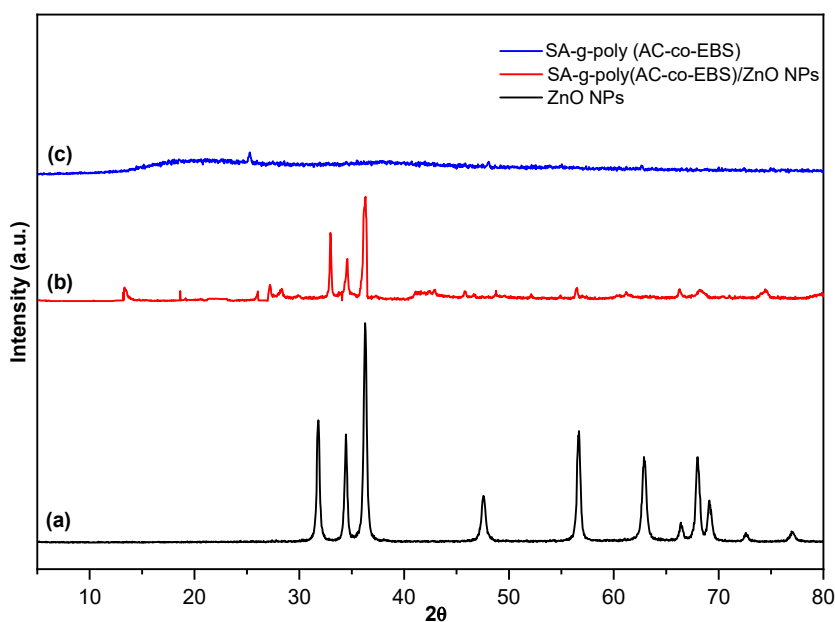


Fig 3. XRD patterns for (a) ZnO NPs according to JCPDS 36-1451, (b) SA-g-poly (Ac-co-EBS)/ZnO, and (c) SA-g-poly (Ac-co-EBS)

variety of amounts of ZnO and a new pattern for nanoparticles due to the strong interaction with the hydrogel and the formation of hydrogen bonds in the SA-g-poly (Ac-co-EBS)/ZnO hydrogel nanocomposite with little shift to a higher angle with the peak appearing at  $33.2^\circ$  [20].

TEM-EDX and FESEM are shown in Fig. 4. In TEM

images of ZnO-loaded SA-g-poly (Ac-co-EBS) hydrogel composite and ZnO NPs. As shown in Fig. 4(a,b), quasi-spherical ZnO NPs with sharp edges were disseminated throughout the hydrogel matrix, as seen in the TEM image. Moreover, the average particle size confirmed for the SA-g-(AC-co-EBS)/ZnO NPs was  $\sim 150$  and  $100 \text{ nm}$  for ZnO NPs with a smooth morphology, where ZnO

NPs observed embedded inside the SA-g-poly (Ac-co-EBS). The incorporation of ZnO NPs into SA-g-poly (Ac-co-EBS) is supported by the presence of zinc and oxygen peaks in the EDX of ZnO-loaded SA-g-poly (Ac-co-EBS) hydrogel composite, as shown in Fig. 4(f) [21]. The synthesized composite includes elements O, C, Zn, Ca, S, and Al, which indicates the presence of ZnO NPs on the ZnO-loading SA-g-poly (Ac-co-EBS) hydrogel composite

[22]. FE-SEM images appear to indicate that the presence of ZnO NPs in the structure of hydrogel contributes to filling hydrogel pores and minimizing the heterogeneous surface. This leads to increased surface texture protuberance and coarseness. The ZnO loading SA-g-poly (Ac-co-EBS) hydrogel composite. After adsorption and loading pollutant TC and PH is extra smooth [15,23-24], as shown in Fig. 4(c-e).

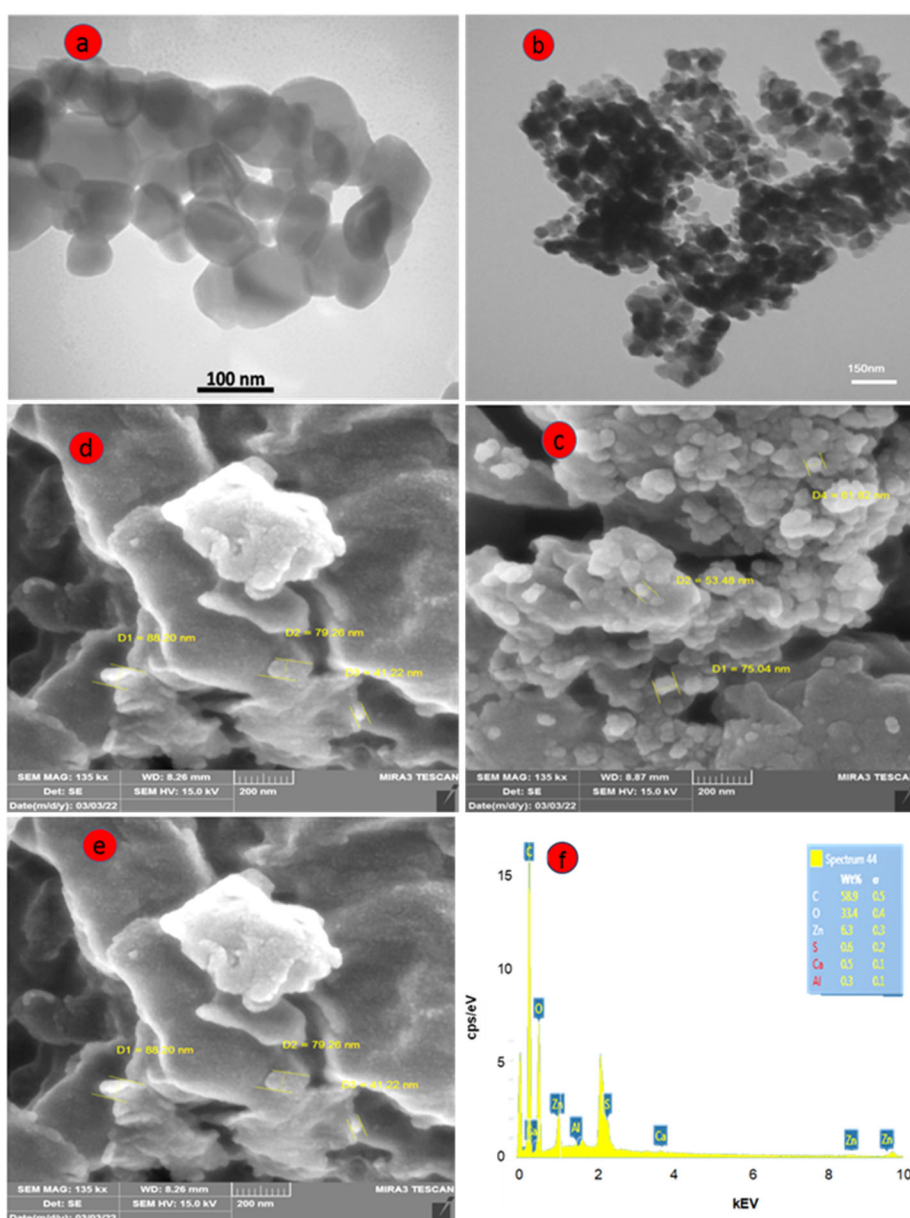


**Fig 4.** TEM images of (a) ZnO NPs and (b) SA-g-(AC-co-EBS)/ZnO NPs. FESEM images of (c) SA-g-(AC-co-EBS)/ZnO NPs, (d) TC loaded SA-g-(AC-co-EBS)/ZnO NPs, (e) PH loaded SA-g-poly (Ac-co-EBS)/ZnO NPs, and (f) EDX of SA-g-(AC-co-EBS)/ZnO NPs

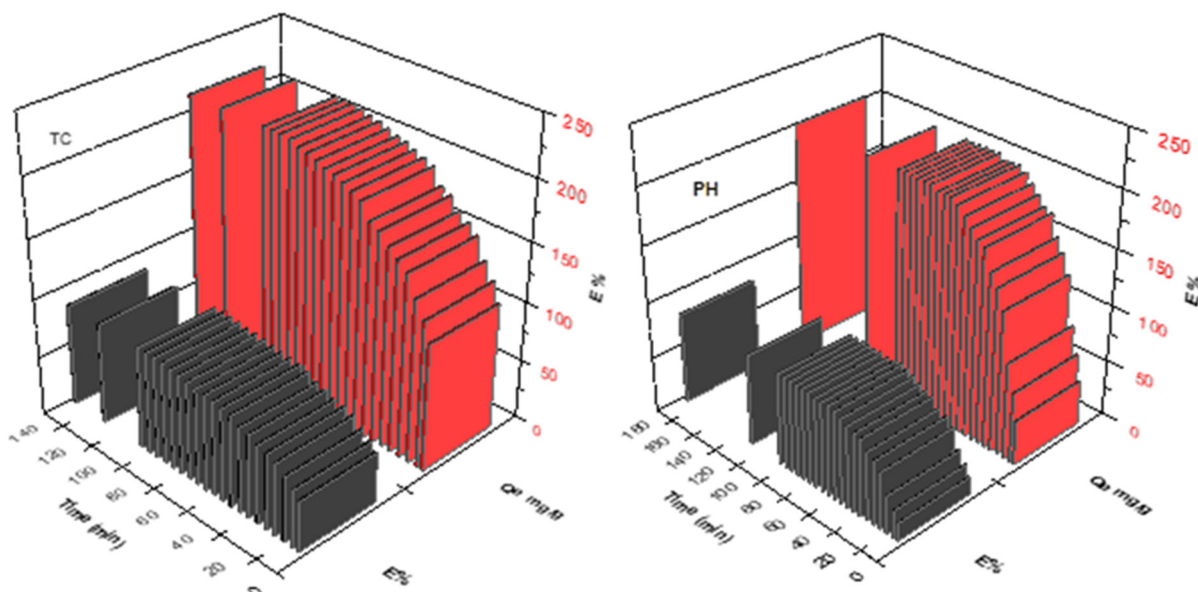


**Fig 5.** Effect of equilibrium time on removal percentage and adsorption efficiency for removal of TC drug and pH by ZnO loading SA-g-poly (Ac-co-EBS)

### Effect of Several Factors on the Adsorption Method for the Removal TC and PH

#### Effect of contact time

The effect of equilibrium time was studied with the initial TC drug and PH concentrations of  $100 \text{ mg L}^{-1}$  at  $30^\circ\text{C}$ . The adsorption efficiency is a function of equilibrium time and primary concentration. The adsorption increased quickly in the first 30 min, and the uptake rate was initially fast until an equilibrium constant value was reached after 2 h of contact. When the initial concentration of TC drug and pH increased to  $100 \text{ mg L}^{-1}$  at  $30^\circ\text{C}$ , the adsorption capacity increased from 106.88 to 215.67 and 79.45 to 203.44 mg/g, while the percentage removal increased from 42.72 to 86.26 and 15.90 to 81.34% at the same order. In the range of higher concentrations of removal, the percentage of removal is lower, while in the range of low concentrations, the percentage of removal of the pollutant is always higher [25]. The results are illustrated in Fig. 5.

#### Mechanism of adsorption

The effect of TC and PH concentrations was studied on the surface prepared by using different concentrations at a temperature of  $25^\circ\text{C}$  and an acidity function ( $\text{pH} = 7.0$ ), and a constant weight of 0.04 g was used for the two surfaces. The results showed that a greater concentration

of pollutants led to an increase in the amount of the adsorbent, and the reason is that the increase in the concentration in the solution will increase the number of adsorbent particles on the surface of the adsorbent, as shown in Fig. 6. It was also noted that the amount of adsorbent for a drug (TC) and the phenolic substance (PH) had very similar values, and the reason for this is that both substances are substances that ionize in the solution into positive charges and negative charges due to the presence of hydroxyl substances in both substances in addition to containing tetracycline, which contains the amine group  $\text{NH}_2$  within its chemical structure. As for the adsorbent surface, SA-g-poly (Ac-co-EBS) contains functional groups such as  $-\text{COOH}$ ,  $\text{OH}$ ,  $\text{C}-\text{O}-\text{C}$ ,  $\text{C}=\text{O}$ , and  $\text{SO}_3$  specific in EBS that are negatively charged in their chemical composition, which will work on hydrogen bonding with the pollutants, as well as the presence of electrostatic interactions between the positive and negative charges of both the surface and the pollutants as shown by Fig. 6, in addition to the  $\pi-\pi$  interferences, as well as van der Waals forces, and thus adsorption will increase [26-27]. The high removal efficiency of TC ( $149 \text{ mg/g}$  at  $\text{pH} = 7$  and  $25^\circ\text{C}$ ) compared with that reported by powdered activated carbon (PAC) and phenolic hydroxyl (bayberry tannin)

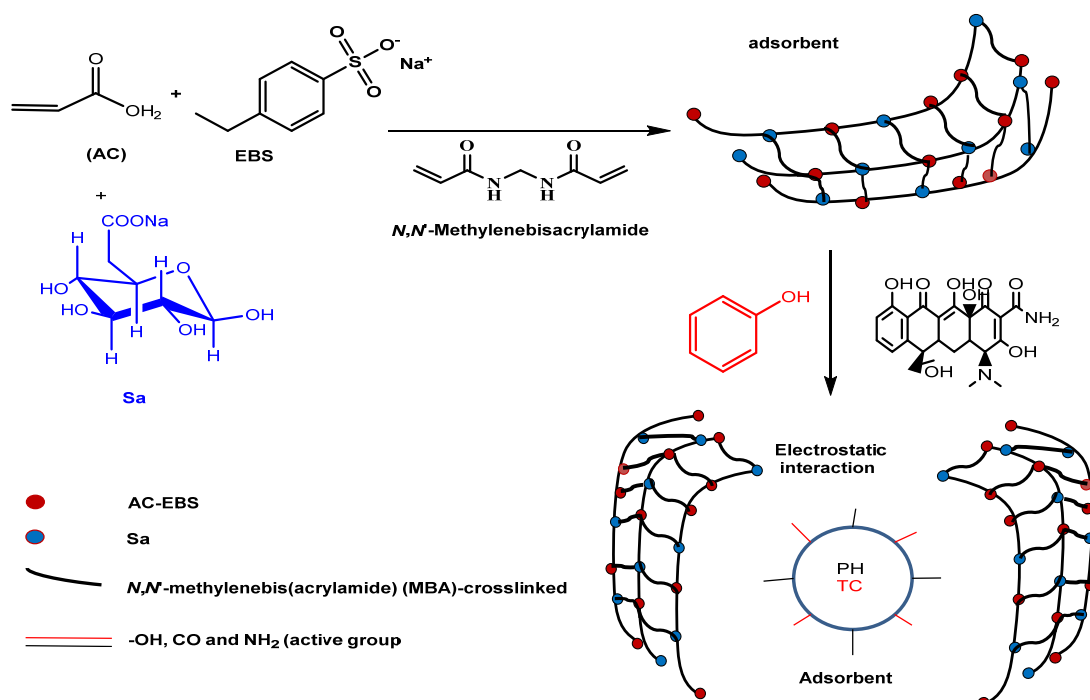


**Fig 6.** The TC and PH adsorption mechanism by SA-g-poly (Ac-co-EBS)

functionalized copper alginate (63 mg/g at pH = 7 and 30 °C) [28-29], It is also compatible kinetically and thermodynamically, and the adsorption process was endothermic and spontaneous. The highest TC removal (90%) was achieved by the rubber waste as an adsorbent, as reported, while the PH adsorption was done by different adsorbents such as metal oxides, ZnO, and coating  $\text{Fe}_3\text{O}_4$  with humic acid 90% capacity, less of 100% and 60 mg/g, respectively [30-32]. In contrast, the capacity of adsorption of SA-g-poly (Ac-co-EBS) for TC and PH was 225 and 215 mg/g at pH = 7 and 30 °C, respectively.

#### Effect of dose of adsorbent

The effect of the quantity of the adsorbents was essential to observing the smallest possible quantity, which shows the maximum adsorption stoichiometry. The quantity of the adsorbent ranged from 0.01–0.10 g/100 mL of ZnO-loaded SA-g-poly (Ac-co-EBS). The results are illustrated in Fig. 7.

The influence of the ZnO loading SA-g-poly (Ac-co-EBS) dosage on the removal percentage of TC drug and PH adsorbed from aqueous solutions showed that increasing the ZnO loading SA-g-poly (Ac-co-EBS)

dosage steadily improved the removal potential of TC drug and PH. Increasing the weight of ZnO loading SA-g-poly (Ac-co-EBS) from 0.01 to 0.10 g was followed by increasing the E% adsorbed from 60.64–97.08% and 48.71–94.05 %. Increasing the masses of SA-g-(AC-co-EBS)/ZnO results in decreasing the removal capacity of the same series of PH from 606.39–97.08 to 487.18–94.46 mg/g at the same order. This is possible because increasing the volume of adsorbent produces a larger surface area or more adsorption sites for pollutants [33-34].

#### Effect of solution pH

The pH solution is one of the essential parameters that have to be accounted for when analyzing the adsorption behavior of sorbate sorbents [35]. The results are illustrated in Fig. 8 around the influence of the initial solution of TC drug at pH 3 to 10 on the adsorption efficiency of TC drug and PH on ZnO loading SA-g-poly (Ac-co-EBS) hydrogel composite. At the optimum conditions of the study ( $500 \text{ mg L}^{-1}$ ), TC drug and PH were adsorbed on 0.04 g ZnO loading SA-g-poly (Ac-co-EBS) for 2 h of equilibrium time and rate shaking 120 rpm. The adsorption capacity for TC drug and PH

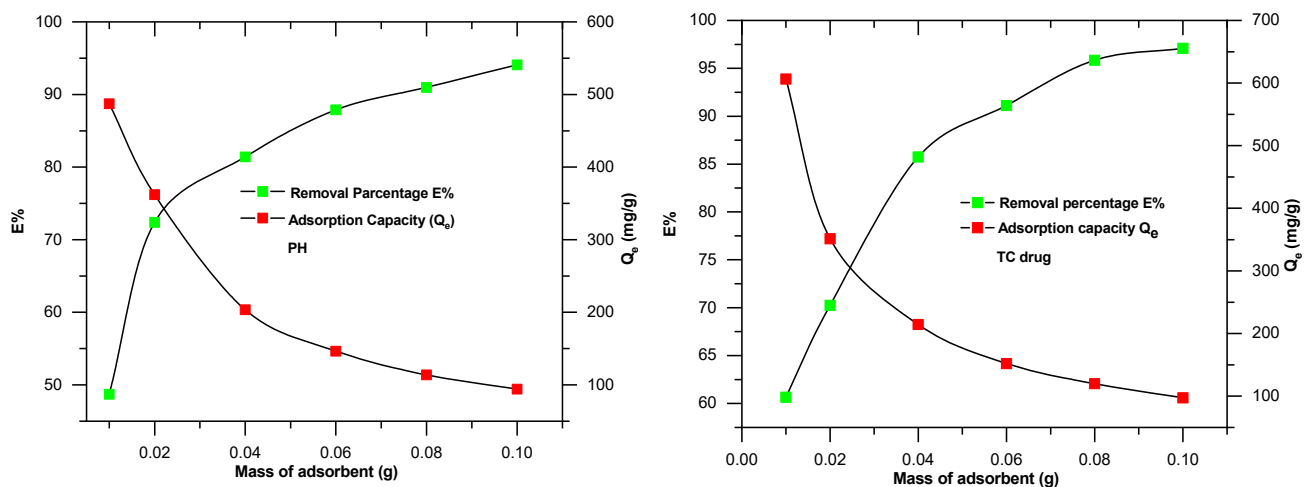


Fig 7. Effect of the amount of adsorbent ZnO loading SA-g-poly (Ac-co-EBS) on the removal E% and adsorption capacity of two pollutants

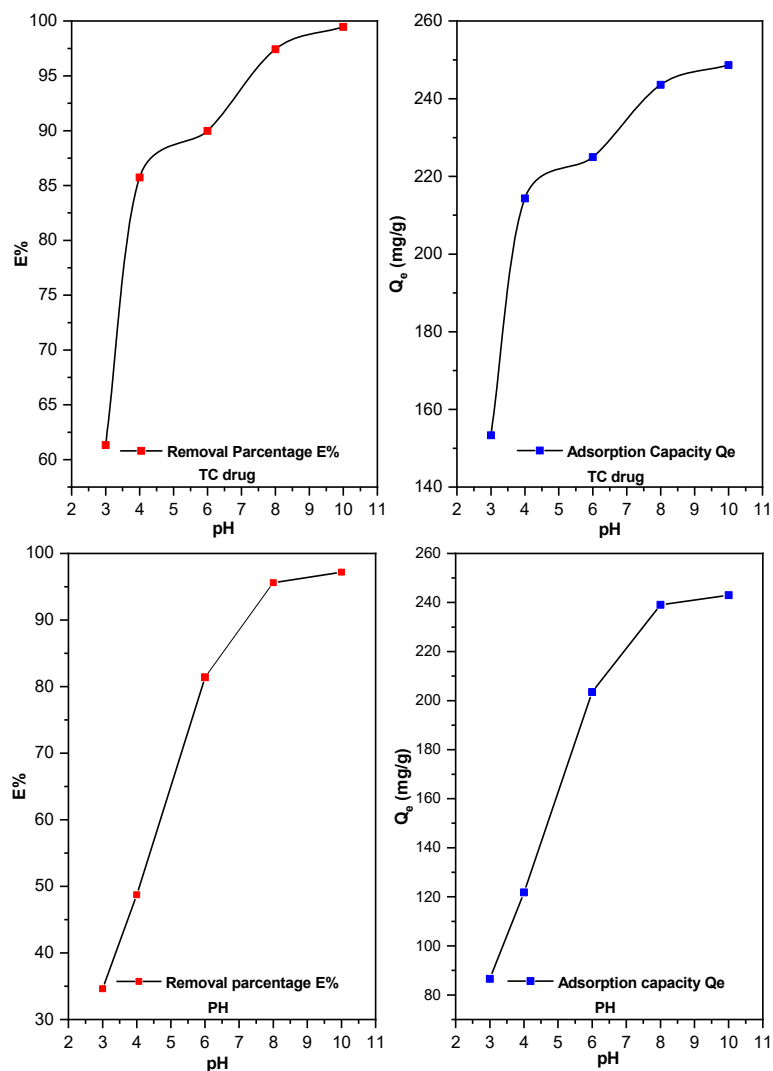


Fig 8. Effect of solution pH on the adsorption of TC drug and PH on ZnO loading SA-g-poly (Ac-co-EBS)

was lowest at pH 3, 153.31 and 86.85 mg/g, respectively; maximum adsorption was achieved [36] at pH 10, 248.66 and 242.95 mg/g at the same order [37]. Where the removal percent for TC drug and PH was lowest at pH 3, i.e., 61.1 and 35%, respectively, and maximum removal was achieved at pH 10, i.e., 99.7 and 97%, respectively. In  $\text{pH} < 7$ , hydrogen ions will be increased in the solution, the adsorbent surface will shrink, and hydrogen bonding will occur between the chains. The surface will be in a state of contraction, indicating the difficulty of diffusion of PH and TC molecules into the surface as well as the occurrence of electrostatic repulsion between the surface and the adsorbent materials, thus reducing adsorption. In  $\text{pH} > 7$ , the  $-\text{COOH}$  and  $-\text{OH}$  groups on the adsorbent and adsorbate surfaces will ionize, lose  $\text{H}^+$ , and become negatively charged groups where the adsorbent surface charge is negative, and electrostatic attraction will occur between the adsorbent surface and the different charged adsorbate molecules, which leads to increased adsorption. In addition to that, repulsion occurs between the negatively charged functional aggregates on the adsorbent surface, swelling, and expansion occur, allowing the adsorbate particles to spread within the adsorbent surface. So, the optimum adsorption conditions for TC and PH were  $\text{pH} > 7$  [38-39].

### Effect of temperature

To limit whether the ongoing adsorption process was exothermic or endothermic in nature. The adsorption

model was estimated for different pollutant-adsorbent methods. The removal of TC drug and PH has been studied at various temperatures (283.15, 293.15, 303.15, and 313.15 K) in the presence of various initial TC drug and PH concentrations 10–100  $\text{mg L}^{-1}$ . Results appear in Fig. 9, the adsorption process increases with increasing temperature, so the adsorption process is endothermic.

In this experimental study, the effect of solution temperature on adsorption will also aid in the calculation of thermodynamic parameters like  $\Delta H$ ,  $\Delta G$ , and  $\Delta S$  of the adsorption method. The equilibrium constant ( $K_e$ ) of the adsorption method at all temperatures was studied from Eq. (2);

$$K_e = \frac{Q_{\max} \times W_t (0.04 \text{ g})}{C_e \times V (0.1 \text{ L})} \times 1000 \quad (2)$$

where  $Q_{\max}$  is the quantity adsorbed in ( $\text{mg g}^{-1}$ ),  $C_e$  equilibrium concentration ( $\text{mg L}^{-1}$ ), 0.04 g mass of the ZnO loading SA-g-poly (Ac-co-EBS) adsorbent, and 0.1 L volume of the solution TC drug PH utilized in the adsorption method. The change free energy can be calculated in Eq. (3) [40];

$$\Delta G = -RT \ln K_e \quad (3)$$

where  $\Delta G$ : Gibbs free energy ( $\text{J K}^{-1} \text{mol}^{-1}$ ),  $T$  is the absolute temperature in Kelvin,  $R$  is the gas constant ( $8.314 \text{ J K}^{-1} \text{mol}^{-1}$ ). The change enthalpy can be calculated in Eq. (4) [41];

$$\ln X_m = -\frac{\Delta H^\circ}{RT} + \text{Cons} \quad (4)$$

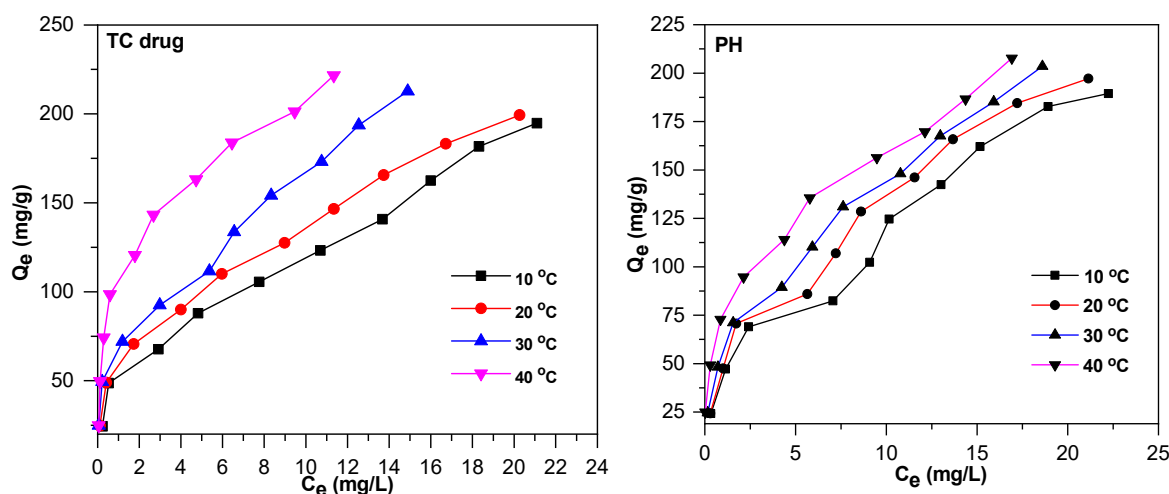


**Fig 9.** Effect of solution temperature on the adsorption of TC drug and PH on the surface of ZnO loading SA-g-poly (Ac-co-EBS), pH 4.6, mass adsorbent 0.04 g/100 mL

where  $X_m$ : is the maximum value of adsorption at a certain value of equilibrium concentration ( $C_e$  mg/L).  $X_m$  values at several temperatures TC drug and PH. Plotting  $\ln X_m$  versus  $(1/T)$  should produce a straight line with a slope  $-\Delta H/R$  as shown in Fig. 10. The values of  $\Delta H$  and  $\Delta S$  can be studied from the slope and intercept, respectively.

The negative  $\Delta G$  value indicates the spontaneity of the adsorption method. The  $\Delta S$  value had been estimated to be large, which indicated an increase in entropy as a result of adsorption [42]. In Table 1, the values  $\Delta H$  of two pollutants are positive, indicating that the adsorption method is endothermic. All adsorption processes are regarded as spontaneous when  $\Delta G$  is negative. The reason for this is that the increase in temperature leads to an increase in the movement of particles due to the increase in kinetic energy resulting from breaking the bond forces between them, as well as an increase in the rate of spread

of the particles adsorbed on the adsorbent surface layer. Also, the surface porosity and pore size increase with increasing temperatures [43].

### Kinetic Models

The mechanism of adsorbate-adsorbent interaction is best described by studying the rate expression for TC and PH adsorption on ZnO loading SA-g-poly (Ac-co-EBS); this can be made known by examining the influence of time on the adsorption method and fitting the experimental findings to several conventional models. Agreed function for model fittings for perfect prediction of experimental results at various times [30]. The rate expression can be determined by analyzing the adsorption result with several kinetic models: the first model, the second model, and the Elovich model (Tables 2 and 3). Description of the adsorption of the kinetic

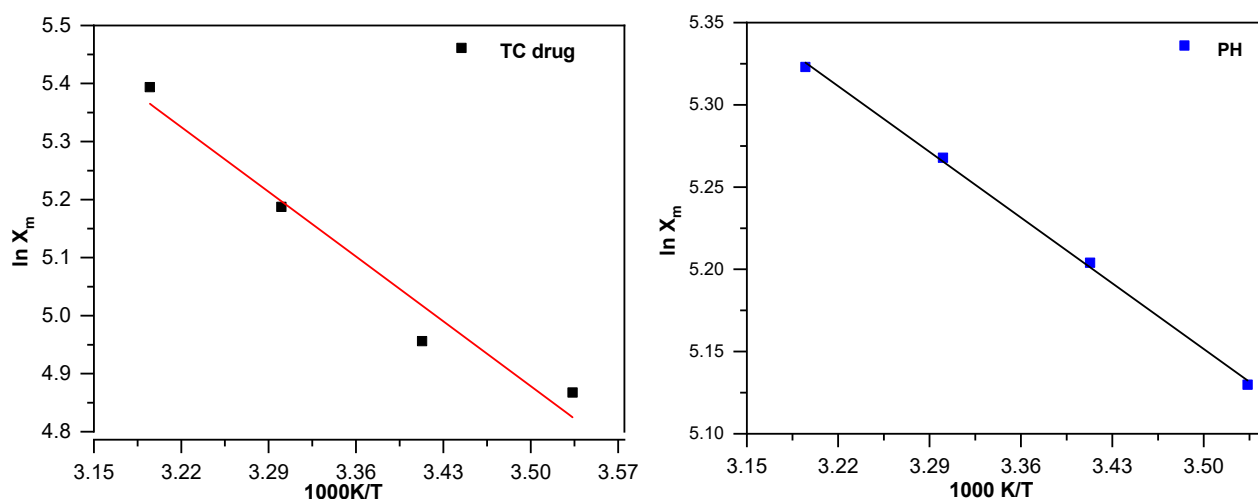


**Fig 10.** Plot  $\ln X_m$  against the absolute temperature of the adsorption TC and PH onto (SA-g-poly (Ac-co-EBS)/ZnO NPs)

**Table 1.** Thermodynamic functions  $\Delta G$ ,  $\Delta S$ , and  $\Delta H$  of TC drug and PH adsorbed on the ZnO loading SA-g-poly (Ac-co-EBS)

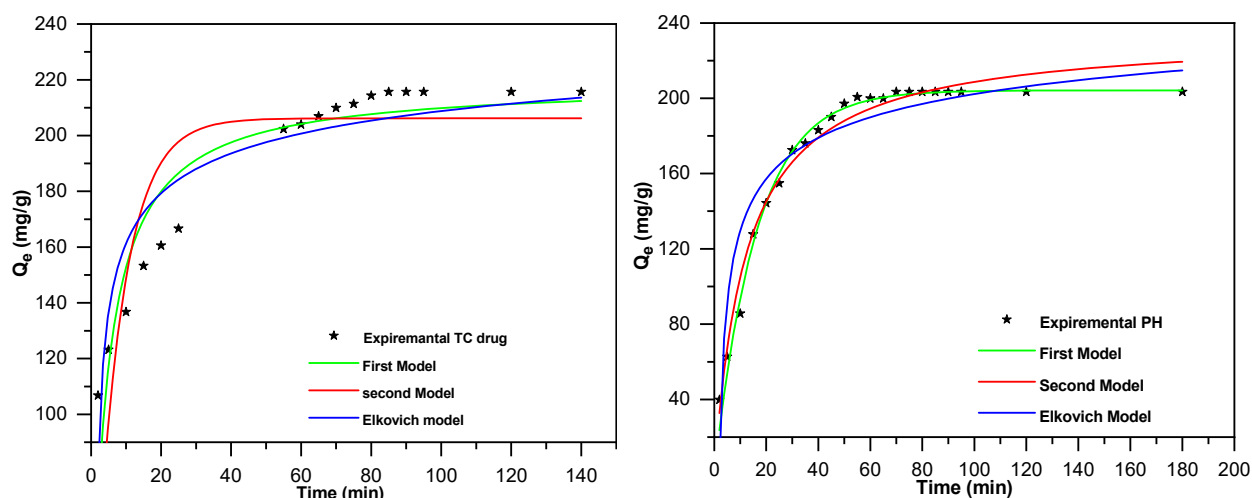
ZnO loading SA-g-poly (Ac-co-EBS) adsorbent									
TC adsorbate					PH adsorbate				
T/K	$K_e$	$-\Delta G$ (kJ mol <sup>-1</sup> )	$\Delta H$ (kJ mol <sup>-1</sup> )	$\Delta S$ (J K <sup>-1</sup> mol <sup>-1</sup> )	T/K	$K_e$	$-\Delta G^\circ$ (kJ mol <sup>-1</sup> )	$\Delta H^\circ$ (kJ mol <sup>-1</sup> )	$\Delta S^\circ$ (J K <sup>-1</sup> mol <sup>-1</sup> )
283.15	11607.14	-22.0213			283.15	9941.176	21.6568		
293.15	12678.57	-23.0145	13.26	86.97275	293.15	10705.88	22.6026	4.742	59.43013
303.15	15982.14	-24.3833			303.15	11411.76	23.5348		
313.15	19642.86	-25.7248			313.15	12058.82	24.4551		

**Table 2.** First-order, second-order, and Elovich including correlation coefficients for TC drug adsorption onto ZnO loading SA-g-poly (Ac-co-EBS)

Kind	Factors	Value	Stand. Error	R <sup>2</sup>
First model	q <sub>e</sub> (mg g <sup>-1</sup> )	206.1850	6.4640	0.9566
	k <sub>f</sub> (min <sup>-1</sup> )	0.1270	0.0233	
Second model	q <sub>e</sub> (mg g <sup>-1</sup> )	218.9540	5.4440	0.8555
	k <sub>s</sub> (g mg <sup>-1</sup> min <sup>-1</sup> )	0.2403	0.0410	
Elovich model	α (mg g <sup>-1</sup> min <sup>-1</sup> )	86.5370	7.0540	0.8123
	β (g min <sup>-1</sup> )	4.5677	1.3010	

**Table 3.** First-order, second-order, and Elovich including correlation coefficients for PH adsorption onto ZnO loading SA-g-poly (Ac-co-EBS)

Kind	Factors	Value	Stand. Error	R <sup>2</sup>
First model	Q <sub>e</sub> (mg g <sup>-1</sup> )	20.4230	1.6308	0.9894
	k <sub>f</sub> (min <sup>-1</sup> )	0.0615	0.0022	
Second model	q <sub>e</sub> (mg g <sup>-1</sup> )	234.4500	4.2560	0.9567
	k <sub>s</sub> (g mg <sup>-1</sup> min <sup>-1</sup> )	0.0810	0.0067	
Elovich model	α (mg g <sup>-1</sup> min <sup>-1</sup> )	104.7920	8.2410	0.8844
	β (g min <sup>-1</sup> )	1.4958	0.1988	

**Fig 11.** Adsorption rate curve kinetic fitted to TC drug and PH adsorption on the ZnO loading SA-g-poly (Ac-co-EBS). (a) first-order; (b) second-order; and (c) Elovich (mass dosage 0.04 g, pH 4.6, Temp. 30 °C)

model the equation first-order calculated in Eq. (5) [44]:

$$q_t = q_e [1 - \exp(-k_f t)] \quad (5)$$

Kinetic model, the equation second-order calculated in Eq. (6) [45].

$$q_t = \frac{K_2 q_e^2 t}{1 + K_2 q_e t} \quad (6)$$

The non-linear model of the chemisorption (Elovich kinetic model) [46] the equation calculates in Eq. (7).

$$q_t = \frac{1}{\beta} \ln \alpha \beta + \frac{1}{\beta} \ln t \quad (7)$$

Further, the kinetic second model has higher correlation coefficients than the first and Elovich models. As a result, adsorption is better suited to the second model than the first and Elovich models. The adsorption of two pollutants onto ZnO-loaded SA-g-poly (Ac-co-EBS) with time shaking 0–240 min and solution initial concentration 500 mg/L. Although the adsorption of pollutants was initially so high, the rate of adsorption slowed over time and progressively reached a constant value, as shown in Fig. 11.

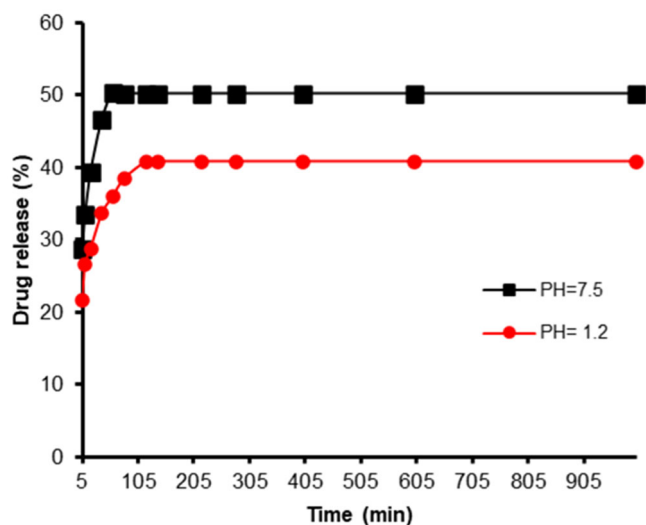


**Fig 12.** Drug release profiles of TC from the ZnO loading SA-g-poly (Ac-co-EBS) in pH 1.2 and pH 7.4 at  $37 \pm 0.5$  °C

### Effect pH on Release Ratio of Tetracycline Drug *In Vitro*

The release of TC was studied in conditions similar to those in the human body in terms of acidity and temperature. It was found that the speed of TC release was higher when the acidity function was higher (pH = 7.5), and this is due to the degree of swelling of the hydrogel and the fact that the dissolution of TC depends on the acidity function. The speed of release of TC in the alkaline medium as a result of the increase in the rate of swelling is greater than in the acidic medium [39]. As for the acid function pH = 1.2, the concentration of  $H^+$  increases, which competes with the unlinked amino group, and thus, the percentage of hydrogel swelling decreases, and thus the percentage of drug release decreases. The initial burst release of 28 and 21.56% in the first hour was observed for TC. The cumulative release of TC in 3 h was 50.65, 42.33% from pH 7.5 and pH 1.2 in the same order as shown in Fig. 12.

### CONCLUSION

The adsorption efficiency and removal efficiency E% of TC and PH rise with increasing equilibrium time, temperature, and surface area. However, adsorption efficiency ( $Q_e$ ) has decreased with the mass increase of the surface. The best equilibrium time for equilibrium to be attained was found to be 2 h. It is essentially due to the

saturation of the active site, which does not allow more adsorption to take place. The adsorption capacity of the TC drug and PH were to rise with an increase in solution pH in the base medium. The negative value of  $\Delta G$  confirms the spontaneous adsorption method. The positive value of  $\Delta S$  illustrated the increased randomness at the solid-solution interface through adsorption, and the positive value of  $\Delta H$  indicated the adsorption method was endothermic. The first model exhibited the best fit for the kinetic studies. The release values of the TC drug from the hydrogel are in the hypothetical bowel fluid pH = 7.5.

### AUTHOR CONTRIBUTIONS

Each of the mentioned authors made a substantial contribution to the creation and writing of this article. Conceived and designed the analysis by Aseel Mushtak Aljeboree; collected the data by Usama Salim Altimari; contributed data or analysis tools by Usama Salim Altimari; verified the analytical methods by Maha Daham Azeez; Mohammed Kassim Al-Hussainawy performed the analysis; writing the paper and the computations by Ashour Hani Dawood and Ayad Fadhil Alkaim.

### REFERENCES

- [1] Abid Alradaa, Z.A., and Kadam, Z.M., 2021, Preparation, characterization and prevention biological pollution of 4 (4-benzophenylazo) pyrogallol and their metal complexes, *IOP Conf. Ser.: Earth Environ. Sci.*, 790, 12038.
- [2] Omran, A.R., Baiee, M.A., Juda, S.A., Salman, J.M., and Alkaim, A.F., 2016, Removal of Congo red dye from aqueous solution using a new adsorbent surface developed from aquatic plant (*Phragmites australis*), *Int. J. ChemTech Res.*, 9 (4), 334–342.
- [3] Mahmoud, M.E., El-Ghanam, A.M., Saad, S.R., and Mohamed, R.H.A., 2020, Promoted removal of metformin hydrochloride anti-diabetic drug from water by fabricated and modified nanobiochar from artichoke leaves, *Sustainable Chem. Pharm.*, 18, 100336.
- [4] Aljeboree, A.M., Alrazzak, N.A., Alqaraguly, M.B., Mahdi, M.A., Jasim, L.S., and Alkaim, A.F., 2020,

- Adsorption of pollutants by using low-cost (environment-friendly): Equilibrium, kinetics and thermodynamic studies: A review, *Sys. Rev. Pharm.*, 11 (12), 1988–1997.
- [5] Yazidi, A., Atrous, M., Edi Soetaredjo, F., Sellaoui, L., Ismadji, S., Erto, A., Bonilla-Petriciolet, A., Luiz Dotto, G., and Ben Lamine, A., 2020, Adsorption of amoxicillin and tetracycline on activated carbon prepared from durian shell in single and binary systems: Experimental study and modeling analysis, *Chem. Eng. J.*, 379, 122320.
- [6] Liu, H., Yang, Y., Sun, H., Zhao, L., and Liu, Y., 2018, Fate of tetracycline in enhanced biological nutrient removal process, *Chemosphere*, 193, 998–1003.
- [7] Hamadneh, I., Abu-Zurayk, R.A., and Al-Dujaili, A.H., 2020, Removal of phenolic compounds from aqueous solution using  $MgCl_2$ -impregnated activated carbons derived from olive husk: The effect of chemical structures, *Water Sci. Technol.*, 81 (11), 2351–2367.
- [8] Khalid Mahmoud, D., Mohd Salleh, M.A., and Wan Abdul Karim, W.A., 2012, Langmuir model application on solid–liquid adsorption using agricultural wastes: Environmental application review, *J. Purity, Util. React. Environ.*, 1 (4), 170–199.
- [9] Xie, J., Li, H., Zhang, T., Song, B., Wang, X., and Gu, Z., 2023, Recent advances in ZnO nanomaterial-mediated biological applications and action mechanisms, *Nanomaterials*, 13 (9), 1500.
- [10] Xin, Z., He, Q., Wang, S., Han, X., Fu, Z., Xu, X., and Zhao, X., 2022, Recent progress in ZnO-based nanostructures for photocatalytic antimicrobial in water treatment: A review, *Appl. Sci.*, 12 (15), 7910.
- [11] Chavhan, J., Rathod, R., Tandon, V., Gupta, S., and Malav, J.K., 2022, Development of EPA/ZnO nanocomposites: Structural, physical, and electrochemical studies, *Surf. Coat. Technol.*, 448, 128846.
- [12] Al-Hussainawy, M.K., Sahb Mehdi, Z., Jasim, K.K., Alshamsi, H.A.H., Saud, H.R., and Kyhoiesh, H.A.K., 2022, A single rapid route synthesis of magnetite/chitosan nanocomposite: Competitive study, *Results Chem.*, 4, 100567.
- [13] Kyhoiesh, H.A.K., Al-Hussainawy, M.K., and Saud, H.R., 2022, Synthesis and characterization of polyacrylamide/crotonic acid and its composites with carbon nanotube and Rhodamine B, *AIP Conf. Proc.*, 2398 (1), 030018.
- [14] Waheeb, A.S., Alshamsi, H.A.H., Al-Hussainawy, M.K., and Saud, H.R., 2020, *Myristica fragrans* shells as potential low cost bio-adsorbent for the efficient removal of rose Bengal from aqueous solution: Characteristic and kinetic study, *Indones. J. Chem.*, 20 (5), 1152–1162.
- [15] Jebur, M.H., Albdere, E.A., Al-Hussainawy, M.K., Alwan, S.H., 2022, Synthesis and characterization of new 1,3-oxazepine-4,7-dione compounds from 1,2-diaminobenzene, *Int. J. Health Sci.*, 6, 4578–4589.
- [16] Oladipo, A.A., and Gazi, M., 2014, Enhanced removal of crystal violet by low cost alginate/acid activated bentonite composite beads: Optimization and modelling using non-linear regression technique, *J. Water Process Eng.*, 2, 43–52.
- [17] Kyhoiesh, H.A.K., Al-Hussainawy, M.K., Waheeb, A.S., and Al-Adilee, K.J., 2021, Synthesis, spectral characterization, lethal dose ( $LD_{50}$ ) and acute toxicity studies of 1,4-bis(imidazolylazo)benzene (BIAB), *Heliyon*, 7 (9), e07969.
- [18] Karim, A.R., and Radia, N.D., 2022, Hydrogel/clay nanocomposites for removal of cationic organic dye from their aqueous solutions, *HIV Nurs.*, 22 (2), 1936–1940.
- [19] Al-Taweel, S.S., Saud, H.R., Kadhum, A.A.H., and Takriff, M.S., 2019, The influence of titanium dioxide nanofiller ratio on morphology and surface properties of  $TiO_2$ /chitosan nanocomposite, *Results Phys.*, 13, 102296.
- [20] Mittal, H., Al Alili, A., Morajkar, P.P., and Alhassan, S.M., 2021, Graphene oxide crosslinked hydrogel nanocomposites of xanthan gum for the adsorption of crystal violet dye, *J. Mol. Liq.*, 323, 115034.
- [21] El Shafey, A.M., Abdel-Latif, M.K., and Abd El-Salam, H.M., 2021, The facile synthesis of poly (acrylate/acrylamide) titanium dioxide nanocomposite for groundwater ammonia removal, *Desalin. Water Treat.*, 212, 61–70.

- [22] Xiong, H.M., Xu, Y., Ren, Q.G., and Xia, Y.Y., 2008, Stable aqueous ZnO@polymer core-shell nanoparticles with tunable photoluminescence and their application in cell imaging, *J. Am. Chem. Soc.*, 130 (24), 7522–7523.
- [23] Badri, N., Chhiti, Y., Bentiss, F., and Bensitel, M., 2020, Synthesis and characterization of vanadium pentoxide on different metal oxides by the sol-gel process for application in the conversion of the SO<sub>2</sub> to SO<sub>3</sub>, *Moroccan J. Chem.*, 8 (3), 560–572.
- [24] Aljeboree, A.M., and Alkaim, A.F., 2019, Comparative removal of three textile dyes from aqueous solutions by adsorption: As a model (corn-cob source waste) of plants role in environmental enhancement, *Plant Arch.*, 19 (1), 1613–1620.
- [25] Wang, F., Zeng, Q., Su, W., Zhang, M., Hou, L., and Wang, Z.L., 2019, Adsorption of bisphenol A on peanut shell biochars: The effects of surfactants, *J. Chem.*, 2019, 2428505.
- [26] Kim, D.G., Boldbaatar, S., and Ko, S.O., 2022, Enhanced adsorption of tetracycline by thermal modification of coconut shell-based activated carbon, *Int. J. Environ. Res. Public Health*, 19 (21), 13741.
- [27] Zhang, X., Lin, X., He, Y., and Luo, X., 2019, Phenolic hydroxyl derived copper alginate microspheres as superior adsorbent for effective adsorption of tetracycline, *Int. J. Biol. Macromol.*, 136, 445–459.
- [28] Dehmani, Y., Dridi, D., Lamhasni, T., Abouarnadasse, S., Chtourou, R., and Lima, E.C., 2022, Review of phenol adsorption on transition metal oxides and other adsorbents, *J. Water Process Eng.*, 49, 102965.
- [29] Dehmani, Y., Lainé, J., Daouli, A., Sellaoui, L., Bonilla-Petriciolet, A., Lamhasni, T., Abouarnadasse, S., and Badawi, M., 2023, Unravelling the adsorption mechanism of phenol on zinc oxide at various coverages via statistical physics, artificial neural network modeling and *ab initio* molecular dynamics, *Chem. Eng. J.*, 452, 139171.
- [30] Koesnarpadi, S., Santosa, S.J., Siswanta, D., and Rusdjarso, B., 2017, Humic acid coated Fe<sub>3</sub>O<sub>4</sub> nanoparticle for phenol sorption, *Indones. J. Chem.*, 17 (2), 274–283.
- [31] Alkaim, A.F., and Aljeboree, A.M., 2020, White marble as an alternative surface for removal of toxic dyes (methylene blue) from aqueous solutions, *Int. J. Adv. Sci. Technol.*, 29 (5), 5470–5479.
- [32] Temel, F., Turkyilmaz, M., and Kucukcongar, S., 2020, Removal of methylene blue from aqueous solutions by silica gel supported calix[4]arene cage: Investigation of adsorption properties, *Eur. Polym. J.*, 125, 109540.
- [33] Tanhaei, B., Ayati, A., Iakovleva, E., and Sillanpää, M., 2020, Efficient carbon interlayered magnetic chitosan adsorbent for anionic dye removal: Synthesis, characterization and adsorption study, *Int. J. Biol. Macromol.*, 164, 3621–3631.
- [34] Liu, X., Wang, L., Zhou, X., He, X., Zhou, M., Jia, K., and Liu, X., 2021, Design of polymer composite-based porous membrane for *in-situ* photocatalytic degradation of adsorbed organic dyes, *J. Phys. Chem. Solids*, 154, 110094.
- [35] Aljeboree, A.M., Alshirifi, A.N., and Alkaim, A.F., 2019, Activated carbon (as a waste plant sources)-clay micro/nanocomposite as effective adsorbent: Process optimization for ultrasound-assisted adsorption removal of amoxicillin drug, *Plant Arch.*, 19 (Suppl. 2), 915–919.
- [36] Chen, L., Ren, X., Alharbi, N.S., and Chen, C., 2021, Fabrication of a novel Co/Ni-MOFs@BiOI composite with boosting photocatalytic degradation of methylene blue under visible light, *J. Environ. Chem. Eng.*, 9 (5), 106194.
- [37] Xu, D., Zhang, Y., Zhang, S., Yang, W., Wang, Z., and Li, J., 2022, Copper nanoleaves SERS substrates with high surface roughness for sensitive detection crystal violet and rhodamine 6G, *Opt. Laser Technol.*, 145, 107502.
- [38] Al-Niaeem, H.S., Abdulwahid, A., and Hanoosh, W., 2022, Preparation of semi IPNs-hydrogel composite for removing Congo red and Bismarck Brown Y from wastewater: Kinetic and thermodynamic study, *Egypt. J. Chem.*, 65 (1), 19–34.
- [39] Osman, A.M., Hendi, A.H., and Saleh, T.A., 2020, Simultaneous adsorption of dye and toxic metal ions using an interfacially polymerized

- silica/polyamide nanocomposite: Kinetic and thermodynamic studies, *J. Mol. Liq.*, 314, 113640.
- [40] Omer, O.S., Hussein, M.A., Hussein, B.H.M., and Mgaidi, A., 2018, Adsorption thermodynamics of cationic dyes (methylene blue and crystal violet) to a natural clay mineral from aqueous solution between 293.15 and 323.15 K, *Arabian J. Chem.*, 11 (5), 615–623.
- [41] Chowdhury, S., Mishra, R., Saha, P., and Kushwaha, P., 2011, Adsorption thermodynamics, kinetics and isosteric heat of adsorption of malachite green onto chemically modified rice husk, *Desalination*, 265 (1-3), 159–168.
- [42] Jan, S.U., Ahmad, A., Khan, A.A., Melhi, S., Ahmad, I., Sun, G., Chen, C.M., and Ahmad, R., 2021, Removal of azo dye from aqueous solution by a low-cost activated carbon prepared from coal: Adsorption kinetics, isotherms study, and DFT simulation, *Environ. Sci. Pollut. Res.*, 28 (8), 10234–10247.
- [43] del Mar Orta, M., Martín, J., Medina-Carrasco, S., Santos, J.L., Aparicio, I., and Alonso, E., 2019, Adsorption of propranolol onto montmorillonite: Kinetic, isotherm and pH studies, *Appl. Clay Sci.*, 173, 107–114.
- [44] Chowdhury, A., Kumari, S., Khan, A.A., Chandra, M.R., and Hussain, S., 2021, Activated carbon loaded with Ni-Co-S nanoparticle for superior adsorption capacity of antibiotics and dye from wastewater: Kinetics and isotherms, *Colloids Surf., A*, 611, 125868.
- [45] Kevadiya, B.D., Joshi, G.V, Mody, H.M., and Bajaj, H.C., 2011, Biopolymer–clay hydrogel composites as drug carrier: Host–guest intercalation and *in vitro* release study of lidocaine hydrochloride, *Appl. Clay Sci.*, 52 (4), 364–367.
- [46] Aguzzi, C., Capra, P., Bonferoni, C., Cerezo, P., Salcedo, I., Sánchez, R., Caramella, C., and Viseras, C., 2010, Chitosan–silicate biocomposites to be used in modified drug release of 5-aminosalicylic acid (5-ASA), *Appl. Clay Sci.*, 50 (1), 106–111.